ATP synthase K^+- and H^+-flux drive ATP synthesis and enable mitochondrial K^+-uniporter function

Magdalena Juhaszova,[1,9] Evgeny Kobrinsky,[1,9] Dmitry B. Zorov,[1,5,9] H. Bradley Nuss,[1] Yael Yaniv,[1] Kenneth W. Fishbein,[2] Rafael de Cabo,[3] Lluis Montoliu,[6] Sandra B. Gabelli,[4,7,8] Miguel A. Aon,[1] Sonia Cortassa,[1] Steven J. Sollott[1,*]

Supplemental Material

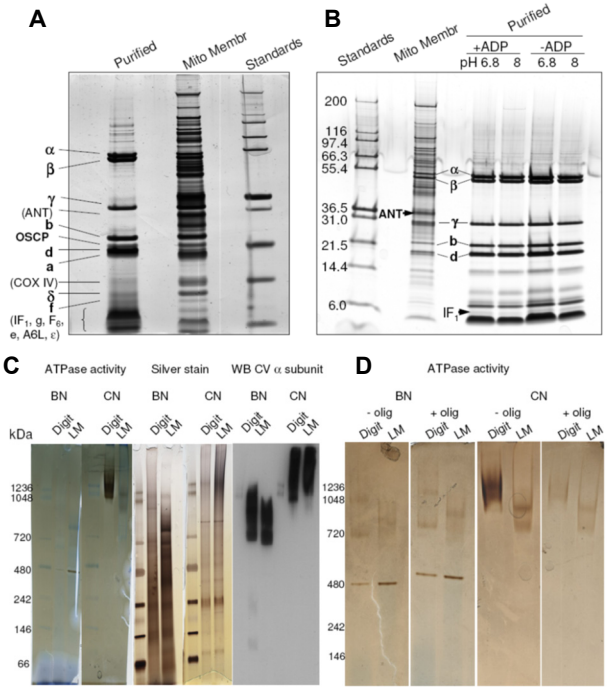

Figure 1 – figure supplement 1. Purity and protein characterization of the isolated F_1F_o complex. F_1F_o was purified according to manufacturer protocol (Mitosciences) and reconstituted into liposomes and planar lipid membranes. The purity of the enzyme complex was assessed by gel electrophoresis, silver staining and Western blotting (under denaturing conditions), which shows the absence of virtually all other unrelated mitochondrial proteins, including ANT, one of the most abundant inner mitochondrial membrane proteins **(A,B)**. It has been suggested that mitochondrial ROMK potassium channel might act as the pore-forming subunit of the cytoprotective mKATP channel (Foster et al, 2012). Our immunoblotting with anti-ROMK antibody eliminated ROMK channel as a contaminant of the isolated F_1F_o (Figure 1-figure supplement 2C). The isolated F_1F_o showed monomers (~720 kD) and dimers (possibly even higher order multimers) when run on Blue- and clear-native gels, although the "in-gel" oligomycin-sensitive ATPase activity, as seen in the clear-native gel, was largely restricted to the dimers and higher **(C,D)**. Note that in the Blue-native gels, the charged dye Coomassie probably interferes with the in-gel ATPase assay. Also, the membrane solubilization detergents digitonin and lauryl maltoside yield different apparent ATPase activities. Importantly, the binding of the small (8 kD) IF_1 to the synthase complex is reversible and pH-dependent, with approximately half of the IF_1 being bound at pH 8 as compared to pH 6.8 **(B)**. The synthase complexes during and after isolation were maintained at pH 7 to keep IF_1 binding, except in protocols for which IF_1 was intentionally removed by a short wash in alkaline (pH 10) buffer.

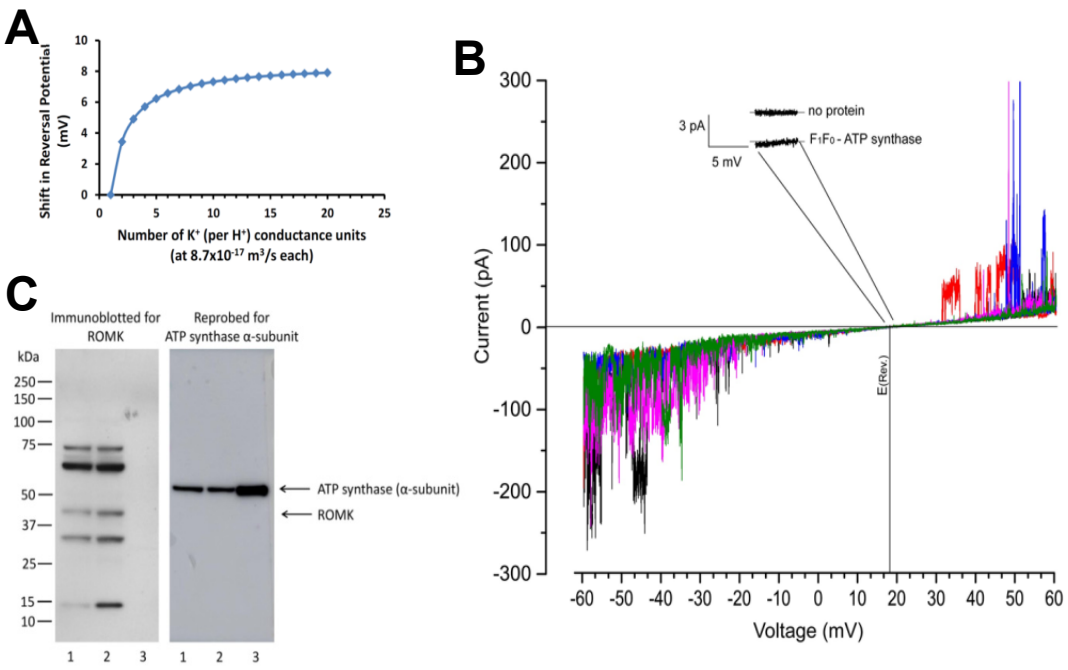

Figure 1 - figure supplement 2. Absence of functionally relevant K^+/H^+ antiport or independent K^+ channel activity contaminating the F_1F_o proteoliposome (PL) reconstitution experiments. (A) Shift in Reversal Potential (E_{rev}) as a function of a hypothetical variation in the stoichiometry of F_1F_o H^+ conductance units vs number of K^+ channels ("K^+ conductance" units)**.** All electrophysiological data confirms the absence of coincidental co-immunoprecipitation with a contaminating K^+ channel (or a Na^+ channel). The results of a calculation based on manuscript equation 1 show a theoretical shift in E_{rev} as a function of a hypothetical variation on the stoichiometry of "H^+ conductance" and "K^+ conductance" units: note that a ratio of 1:1 yields the obtained E_{rev} in the present experiments (a ratio of 1:0 represents the absence of a "K^+ conductance unit" and E_{rev} will equal the reversal potential for H^+ which is set by ionic conditions to be zero; this result has never been seen in any of our experiments). A ratio of 2:1 means two "K^+ conductance" units per "H^+ conductance", and so on. If purified F_1F_o complex displayed a 2:1 ratio we would observe a ~3.5 mV positive shift in E_{rev}, which was never observed. That E_{rev} is invariant from experiment to experiment (our resolution is < 1 mV) confirms a fixed 1:1 stoichiometry. Furthermore, the K^+ conductance is quantitatively inhibited in parallel with that of H^+, without any shifts in E_{rev}, by the titration with ATP (Figure 6D). Finally, the "H^+ conductance" and "K^+ conductance" units are all completely inhibited by both Oligo and Vent. If there was a contaminating K^+ (or Na^+) channel co-immunoprecipitated with F_1F_o, that channel activity would remain after these inhibitors, as we know of no K^+ (or Na^+) channels that are coincidentally *fully* sensitive and inhibited by Oligo and Vent, but such a residual channel activity never happens. Additionally, given the apparent 1:1 stoichiometry with F_1F_o of such a hypothetical K^+ (or Na^+) channel, its abundance should be similar, for example, to the γ-subunit, but there is no such unidentified band of similar abundance in silver-stained gels run on the immunoprecipitated F_1F_o used in the present experiments (**Figure 1 - figure supplement 1**).

(B) Biophysical evidence ruling out contamination of different K^+ channels separate and distinct from F_1F_o. Currents were recorded in F_1F_o-reconstituted bilayers in the voltage-ramp mode. Five random examples of the voltage-ramp data are given (depicted in different colors). Inset shows the current noise amplitude around E_{rev} with reconstituted F_1F_o which remains identical to that without reconstituted proteins. In the hypothetical scenario of the presence of a separate K^+ channel distinct from F_1F_o, the noise amplitude at E_{rev} created by the continuous, independent channel-gating activities of the two putative independent channels (whose time-averaged currents exact summate to zero at E_{rev}) would be significantly larger than pure bilayer noise, and distinct from F_1F_o. In contrast, if ions entering and turning the F_1F_o c-ring are sharing the common path for both K^+ and H^+ permeation, independent gating would not occur - there would be no channel-gating activity at all at E_{rev} – therefore, the noise amplitude at E_{rev} would be equivalent to that of the plain bilayer without reconstituted proteins. The absence of any channel-gating at E_{rev} (Figure inset) rules out the possibility that K^+ is being conducted by a separate K^+ channel co-immunoprecipitated with F_1F_o.

(C) Immunocaptured F_1F_o is devoid of contamination with ATP-dependent ROMK potassium channel. Immunoblot analysis of rat heart mitochondria (10 µg; lane 1), left ventricle tissue lysate (10 µg; lane 2) and immunocapture purified rat heart F_1F_o (~5 µg) separated on a NuPage 4-12% Bis-Tris gel prior to immunoblot assay and tested with anti-KCNJ1 (Sigma Prestige, anti-KCNJ1 Cat#:HPA026962; this antibody has been employed to identify mitochondrial ROMK channel by (Foster et al, 2012)), the blot was then re-probed with anti-ATP synthase subunit α antibody. Arrows point to location of the ROMK channel and the ATP synthase subunit α. While left ventricle and cardiac mitochondria extracts showed the expected weak but positive band ~45 kDa, there was no immunolabelling whatsoever in our F_1F_o complex. Thus there is no ROMK contaminating our preparations to yield any functional artefact.

Supplementary file 1
Quantitative comparison of H^+ and K^+ current magnitudes through ATP synthase

To compute the ratio of H^+ and K^+ currents through the ATP synthase we consider the contribution of each ion as described by the Goldman-Hodgkin-Katz formalism:

$$\frac{I_{H^+}}{I_{K^+}} = \frac{P_H Z_H{}^2 \frac{\Delta\Psi_m F^2}{RT}\left(\frac{[H]_i - [H]_0 \exp\left(\frac{-Z_H \Delta\Psi_m F}{RT}\right)}{1-\exp\left(\frac{-Z_H \Delta\Psi_m F}{RT}\right)}\right)}{P_K Z_K{}^2 \frac{\Delta\Psi_m F^2}{RT}\left(\frac{[K]_i - [K]_0 \exp\left(\frac{-Z_K \Delta\Psi_m F}{RT}\right)}{1-\exp\left(\frac{-Z_K \Delta\Psi_m F}{RT}\right)}\right)}$$

Taking the limit of the ratio of currents when $\Delta\Psi_m$ tends to - ∞, i.e., in the direction of ATP synthesis,

$$\lim_{\Delta\Psi_m \to -\infty}\left(\frac{I_{H^+}}{I_{K^+}}\right) = \frac{P_H Z_H{}^2 \left(\frac{[H]_i - [H]_0 \exp\left(\frac{Z_H \infty F}{RT}\right)}{1-\exp\left(\frac{Z_H \infty F}{RT}\right)}\right)}{P_K Z_K{}^2 \left(\frac{[K]_i - [K]_0 \exp\left(\frac{Z_K \infty F}{RT}\right)}{1-\exp\left(\frac{Z_K \infty F}{RT}\right)}\right)}$$

the linear terms ($[H]_i$, $[K]_i$ and the 1 in the numerators and denominators, respectively), become negligible with respect to the exponential terms containing the dependence on $\Delta\Psi_m$ as follows:

$$\lim_{\Delta\Psi_m \to -\infty}\left(\frac{I_{H^+}}{I_{K^+}}\right) = \frac{P_H Z_H{}^2 \left(\frac{\cancel{[H]_i} - [H]_0 \exp\left(\frac{Z_H \infty F}{RT}\right)}{\cancel{1}-\exp\left(\frac{Z_H \infty F}{RT}\right)}\right)}{P_K Z_K{}^2 \left(\frac{\cancel{[K]_i} - [K]_0 \exp\left(\frac{Z_K \infty F}{RT}\right)}{\cancel{1}-\exp\left(\frac{Z_K \infty F}{RT}\right)}\right)}$$

rendering

$$\lim_{\Delta\Psi_m \to -\infty}\left(\frac{I_{H^+}}{I_{K^+}}\right) = \frac{P_H Z_H{}^2 [H^+]_0}{P_K Z_K{}^2 [K^+]_0}$$

This limit will be (asymptotically) approached as the magnitude of $\Delta\Psi_m$ increases, but under realistic ionic conditions, is practically achieved for $|\Delta\Psi_m| \geq 100$ mV. The currents ratio through ATP synthase will be proportional to the ratio of extra-mitochondrial concentrations (in mole-equivalents) of $[H^+] = 6.3\times10^{-8}$ over $[K^+] = 0.137$, at pH 7.2, corresponding to $\sim 5\times10^{-7} : 1$. This results in a ratio of H^+: K^+ currents ~ 1:4 since the ratio of permeability P_H:P_K is equal to $5.2\pm0.9 \times10^{-11} : 8.7\pm2.9 \times10^{-17}$ as determined in our experiments.

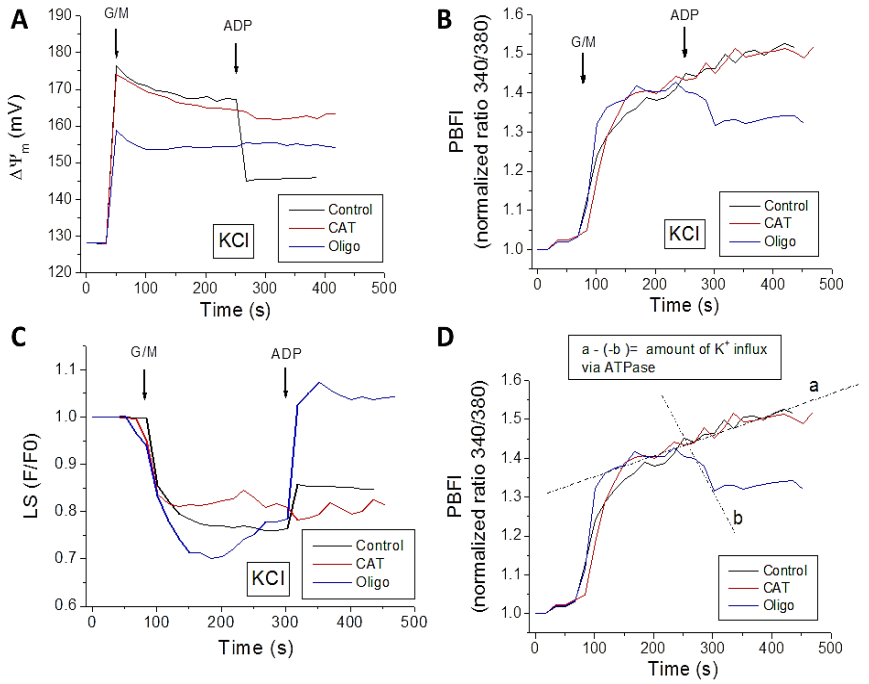

Figure 4 - figure supplement 1. K^+ fluxes during the state 4 → 3 transition in isolated mitochondria from guinea pig heart. Freshly isolated mitochondria loaded with 20 µM PBFI-AM as described before (Aon et al, 2010) were preincubated in the absence (Control) or presence of 10 µM oligomycin (Oligo) or 10 µM carboxyatractyloside (CAT) (in the cuvette of the spectrofluorimeter, with stirring at 37ºC for 3min) followed by energization with the Na^+ salts of substrates glutamate/malate (G/M, 5 mM/5 mM) (state 4 respiration) and, subsequently, with 1mM ADP (state 3 respiration), added as indicated with arrows. Mitochondria were assayed in the same medium above described containing 137 mM KCl (instead of sucrose) and 2 mM Pi. Mitochondrial $\Delta\Psi_m$ (A), PBFI (B) and swelling (light scattering, LS) (C), were monitored simultaneously as described above. (C, D) Volume changes during mitochondrial swelling-contraction, and of the K^+ flux sustained by the ATP synthase in state 3 respiration, were estimated in control and oligomycin-preincubated mitochondria. The relative volume changes (measured as LS) were: *swelling* triggered by G/M (~ 0.3 for Oligo and ~0.2 for control and carboxyatractyloside, CAT), and *contraction* by ADP (~ 0.1 for control and ~ 0.3 for Oligo) additions (C). On these bases, the volume change quantification can be estimated considering that 1.77 µl/mg mitochondrial protein (see (Aon et al, 2010) p.75, 2nd column, 2nd paragraph) correspond to the volume in state 4 respiration after G/M addition. A Δvolume of 30% contraction after ADP addition can be estimated equivalent to 0.5 µl/mg mito prot., thus from 1.77 to 1.24 µl/mg mito protein, sustained by a K^+ flux equivalent to 60% of the K^+ flux at V_{max}.
(D) Estimation of the K^+ flux sustained by the ATP synthase in state 3 respiration in the presence of Oligo: In KCl, V_{max} of K^+ uptake rate = 172±17 nmol K^+/min/mg prot. (see Aon et al., 2010, their Figure 2A).
Slopes (PBFI ratio/min) = Control: 0.00102; +Oligo: - 0.00169
dK^+/dt = influx – efflux = flux balance from control.
Flux balance from control + efflux = influx
0.00102 + 0.00169 = 0.00271 PBFI ratio/min = 0.0183 PBFI ratio/min/mg prot. (148 µg mitochondrial prot. per assay)
K^+ flux = 0.0183 * 1000/0.175 = 104 nmol K^+/min/mg prot.
For a V_{max} uptake rate of K^+ = 172 nmol/min/mg prot.; 104 nmol K^+/min/mg prot. represents 60% of the total K^+ flux at V_{max}.

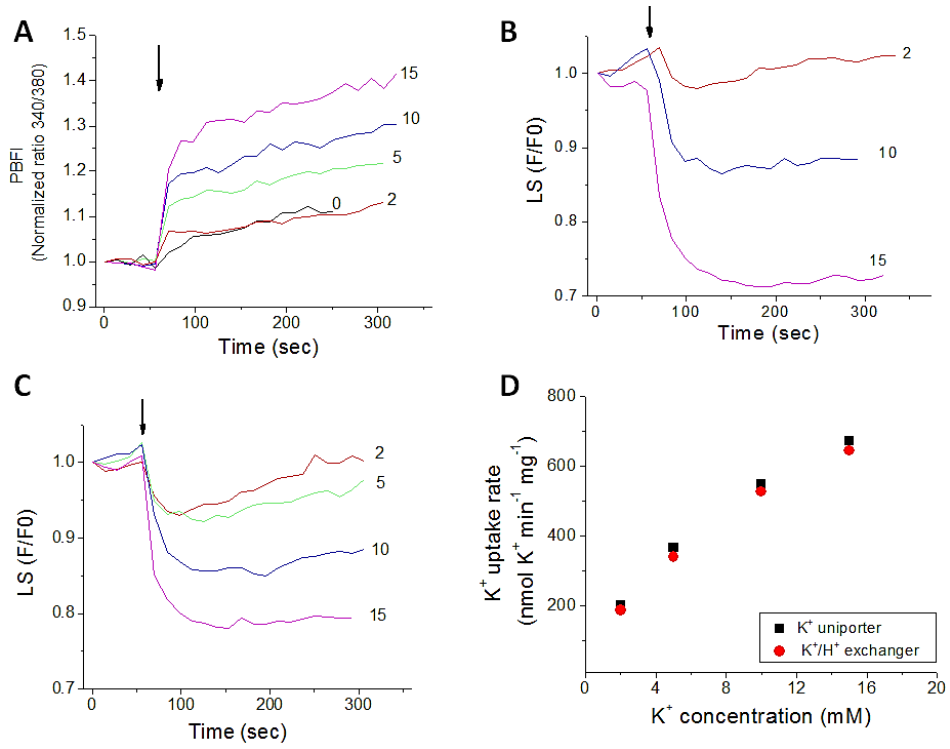

Figure 4 - figure supplement 2. K^+ uniporter and K^+/H^+ exchanger fluxes in the absence or presence of quinine in isolated mitochondria from guinea pig heart.

Freshly isolated PBFI-loaded mitochondria were assayed for K^+ fluxes in the same medium described in the legend of Figure 4 - figure supplement 1, but containing 250 mM sucrose (instead of KCl), thus enabling us to study K^+ fluxes in a controlled fashion. After pulses of 2 to 15 mM KH_2PO_4 (indicated by arrow), K^+ fluxes were quantified in mitochondria energized with the Na^+ salts of G/M (5 mM/5 mM), and in the absence (Control) or presence of 50 µM quinine, a K^+/H^+ exchanger inhibitor (Garlid et al, 1986; Martin et al, 1986). Mitochondrial swelling (LS: B, C) and PBFI fluorescence (A) were determined in control (B) and quinine-preincubated (A, C) mitochondria. Panel D depicts the K^+ fluxes sustained by the K^+ uniporter and the K^+/H^+ exchanger as measured in the presence of quinine or its absence, respectively. The flux through the K^+/H^+ exchanger was calculated as the difference between the fluxes measured in the presence of quinine (uniporter) minus in its absence (where both uniporter and exchanger are active).

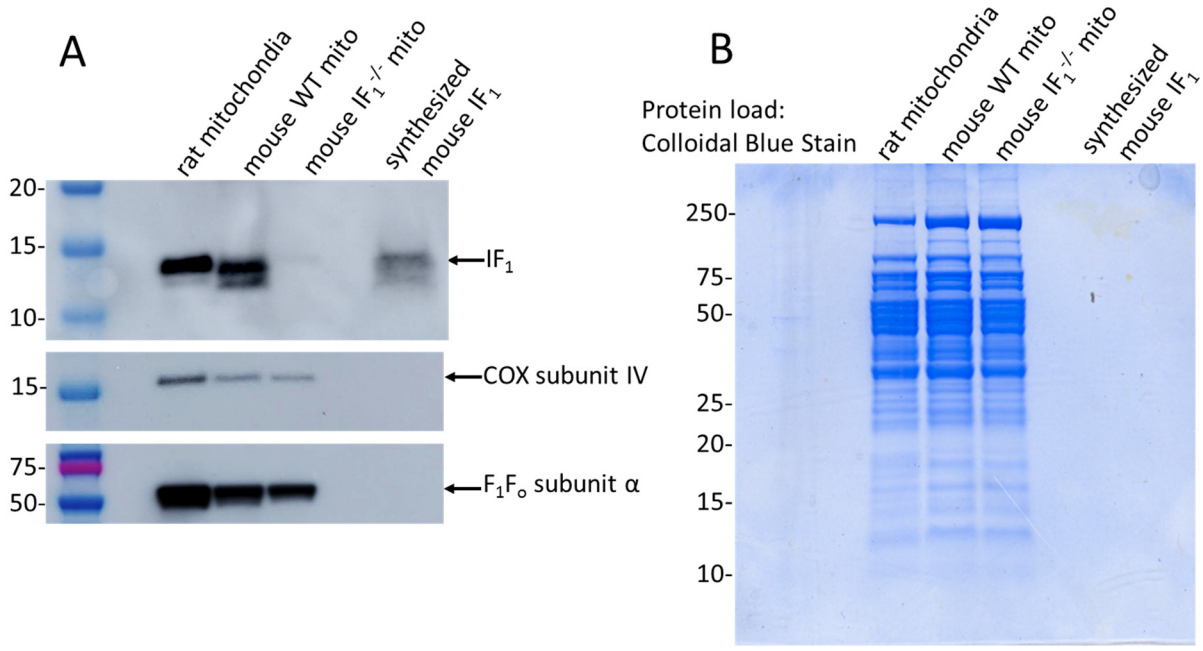

Figure 5D-figure supplement 1. Phenotype verification of IF_1 KO mouse. **A.** IF_1 protein expression was not detected by an anti-IF_1 antibody (Cell Signaling Technology) in $IF_1^{-/-}$ mouse mitochondria by western blotting while the blot was positive for IF_1 protein expresion in rat and mouse wild type (WT) mitochondria (15 µg of proteins were loaded per well) and synthetized mouse IF_1 peptide (purified >98%; 50 ng). As expected, all three mitochondrial preparations showed the presence of other mitochondrial proteins (the same blot was reprobed for COX subunit IV (Cell Signaling Technology, clone 3E11) and F_1F_o subunit alpha (Abcam). **B.** The gel was stained with Colloidal Blue Stain (Invitrogen) to demonstrate the equal total mitochondrial protein load into each well.

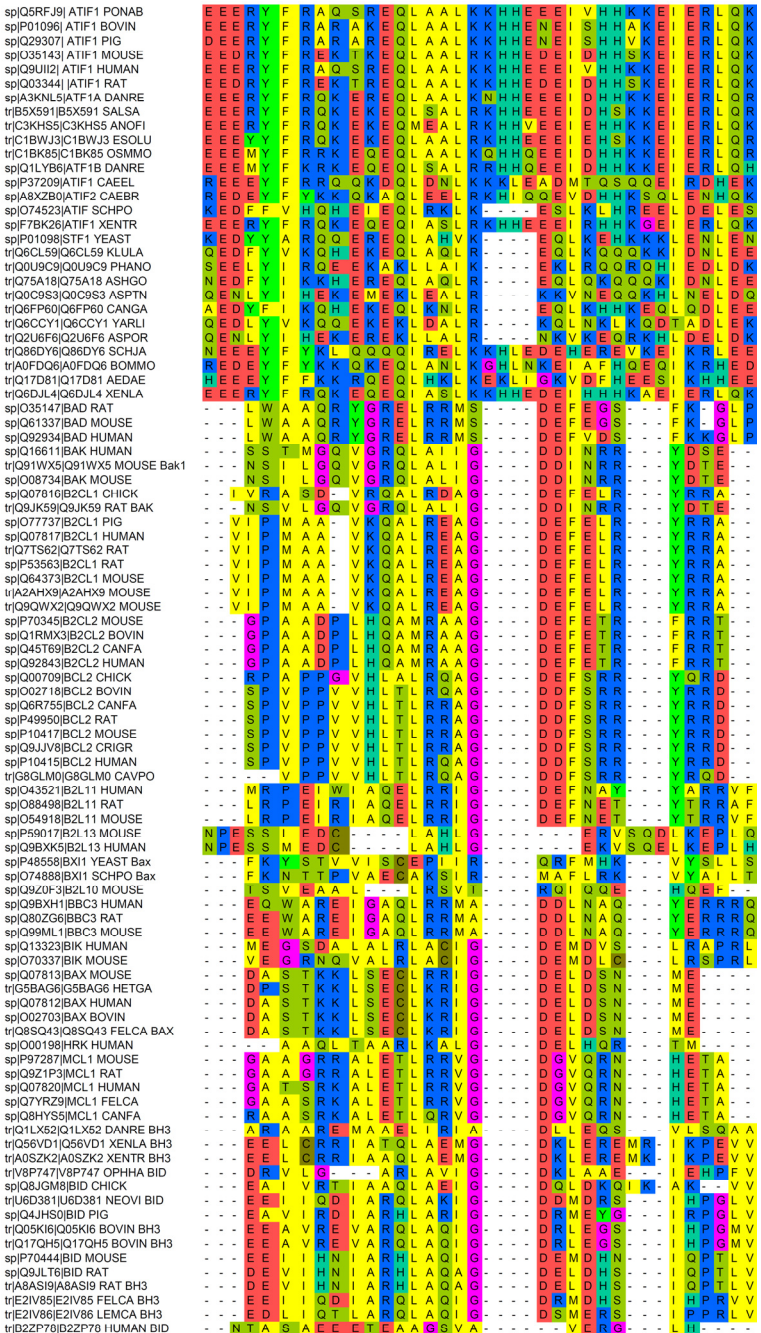

Figure 8 - figure supplement 1. Multiple sequence alignment of BH3 motifs of Bcl-2 proteins and IF1.
The alignment was obtained with Clustal Omega. Details of the 107 sequences corresponding to fragments of the IF1 (28 correspond to IF1 sequences) and Bcl-2 family proteins are provided in Figure 8-Table supplement 1.

.

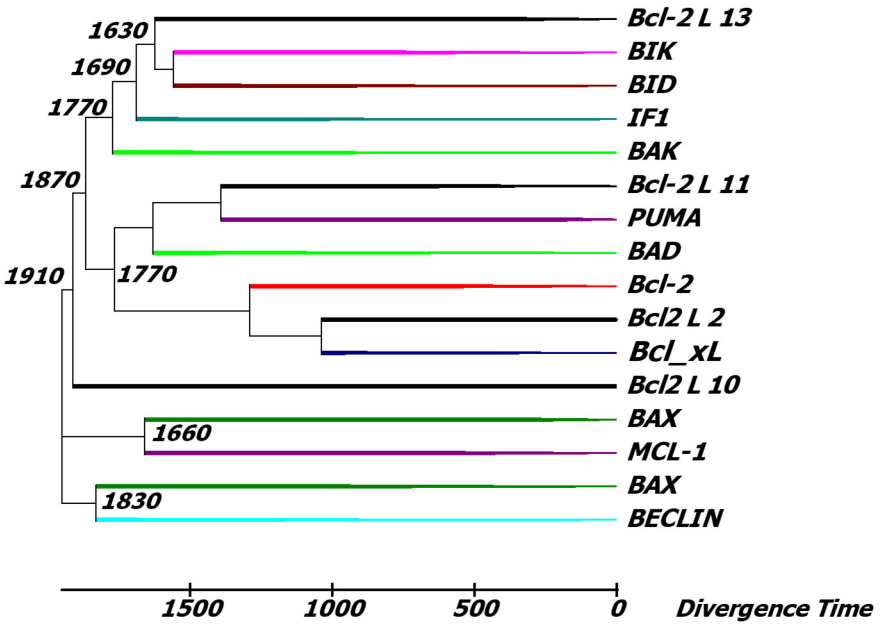

Figure 8-figure supplement 2. Phylogenetic tree of IF1 and BH3 motif containing proteins.
The tree was calculated with the Neighbor-Joining statistical method (Saitou & Nei, 1987) from the alignment performed by Clustal Omega (Figure 8-figure supplement 1). The calibration of the divergence times (in millions of years, Myr) was performed as described in Methods and to calculate the branching times the method RelTime (Tamura et al, 2012) was applied. Only positions with more than 95% site coverage were considered for the analysis, which in this case corresponds to 14 amino acids. The tree construction was performed with MEGA 6.0 (Tamura et al, 2013)

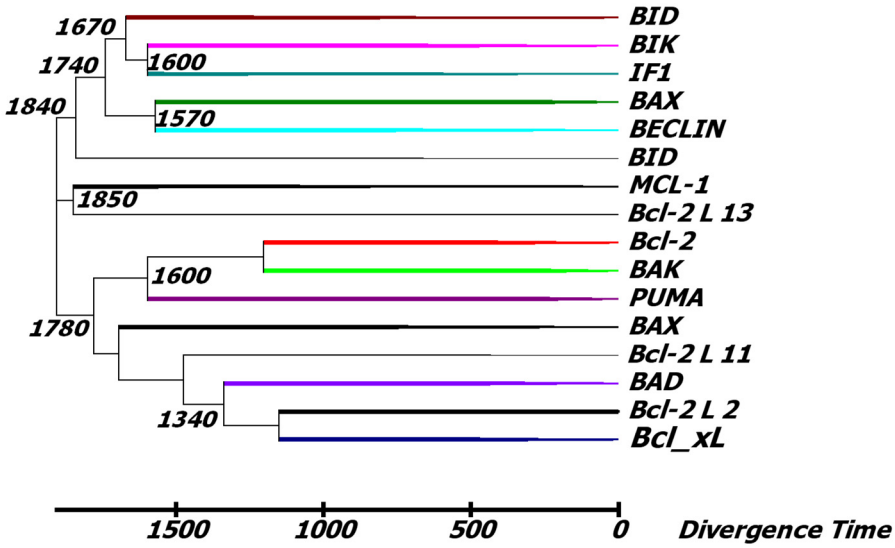

Figure 8-figure supplement 3. Phylogenetic tree of IF1 and Bcl-2 protein BH3 motif containing fragments. The tree was calculated with the Neighbor-Joining statistical method from the alignment performed by Bali-Phy with a LG substitution model (Le & Gascuel, 2008) and the Insertion/deletion model RS07 (Redelings & Suchard, 2007). The calibration of the divergence times was performed as described in methods and to calculate the branching times the method RelTime was applied. Only positions with more than 95% site coverage were considered for the analysis, which in this case corresponds to 9 residues. The tree construction was performed with MEGA 6.0. The bootstrap consensus tree obtained in Mega 6.0 was very similar to that calculated by the joint estimation of Bali-phy.

Figure 8-Table 1

Key for the input sequences used in the phylogenetic analysis

sp|Q1LYB6|ATF1B	DANRE	ATIF1	*Danio rerio*
sp|A3KNL5|ATF1A	DANRE	ATIF1	*Danio rerio*
sp|P01096|ATIF1	BOVIN	ATIF1	*Bos Taurus*
sp|P37209|ATIF1	CAEEL	ATIF1	*Caenorhabditis elegans*
sp|Q9UII2|ATIF1	HUMAN	ATIF1	*Homo sapiens*
sp|Q5RFJ9|ATIF1	PONAB	ATIF1	*Pongo abelii*
sp|A8XZB0|ATIF2	CAEBR	ATIF1	*Caenorhabditis briggsae*
sp|O74523|ATIF	SCHPO	ATIF1	*Schizosaccharomyces pombe*
sp|Q03344|ATIF1	RAT	ATIF1	*Rattus norvegicus*
sp|F7BK26|ATIF1	XENTR	ATIF1	*Xenopus tropicalis*
sp|Q29307|ATIF1	PIG	ATIF1	*Sus scrofa*
sp|O35143|ATIF1	MOUSE	ATIF1	*Mus musculus*
sp|P01098|STF1	YEAST	Putative ATPase inhibitor	*Saccharomyces cerevisiae*
tr|Q6CL59|Q6CL59	KLULA	Putative ATPase inhibitor	*Kluyveromyces lactis*
tr|Q0U9C9|Q0U9C9	PHANO	Putative ATPase inhibitor	*Phaeosphaeria nodorum*
tr|Q75A18|Q75A18	ASHGO	Putative ATPase inhibitor	*Ashbya gossypii*
tr|Q0C9S3|Q0C9S3	ASPTN	Putative ATPase inhibitor	*Aspergillus terreus*
tr|Q6FP60|Q6FP60	CANGA	Putative ATPase inhibitor	*Candida glabrata*
tr|Q6CCY1|Q6CCY1	YARLI	Putative ATPase inhibitor	*Yarrowia lipolytica*
tr|Q2U6F6|Q2U6F6	ASPOR	Putative ATPase inhibitor	*Aspergillus oryzae*
tr|Q86DY6|Q86DY6	SCHJA	Putative ATPase inhibitor	*Schistosoma japonicum*
tr|A0FDQ6|A0FDQ6	BOMMO	ATIF1	*Bombyx mori*
tr|Q17D81|Q17D81	AEDAE	Putative ATPase inhibitor	*Aedes aegypti*
tr|B5X591|B5X591	SALSA	ATIF1	*Salmo salar*
tr|C1BWJ3|C1BWJ3	ESOLU	ATIF1	*Esox Lucius*
tr|C3KHS5|C3KHS5	ANOFI	ATIF1	*Anoplopoma fimbria*
tr|C1BK85|C1BK85	OSMMO	ATIF1	*Osmerus mordax*
tr|Q6DJL4|Q6DJL4	XENLA	atpif1	*Xenopus laevis*
sp|Q16611|BAK	HUMAN	BAK1	*Homo sapiens*
tr|Q91WX5|Q91WX5	MOUSE	Bak1	*Mus musculus*
sp|O08734|BAK	MOUSE	Bak1	*Mus musculus*
sp|Q07816|B2CL1	CHICK	BCL2L1	*Gallus gallus*
tr|Q9JK59|Q9JK59	RAT	Bak1	*Rattus norvegicus*
sp|O77737|B2CL1	PIG	BCL2L1	*Sus scrofa*
sp|Q07817|B2CL1	HUMAN	BCL2L1	*Homo sapiens*
tr|Q7TS62|Q7TS62	RAT	Bcl2l1	*Rattus norvegicus*
sp|P53563|B2CL1	RAT	Bcl2l1	*Rattus norvegicus*
sp|Q64373|B2CL1	MOUSE	Bcl2l1	*Mus musculus*
tr|A2AHX9|A2AHX9	MOUSE	Bcl2l1	*Mus musculus*
tr|Q9QWX2|Q9QWX2	MOUSE	Bcl2l1	*Mus musculus*
sp|P70345|B2CL2	MOUSE	Bcl2l2	*Mus musculus*

sp|Q1RMX3|B2CL2	BOVIN	BCL2L2	*Bos Taurus*
sp|Q45T69|B2CL2	CANFA	BCL2L2	*Canis familiaris*
sp|Q92843|B2CL2	HUMAN	BCL2L2	*Homo sapiens*
sp|Q00709|BCL2	CHICK	BCL2	*Gallus gallus*
sp|O02718|BCL2	BOVIN	BCL2	*Bos Taurus*
sp|Q6R755|BCL2	CANFA	BCL2	*Canis familiaris*
sp|P49950|BCL2	RAT	Bcl2	*Rattus norvegicus*
sp|P10417|BCL2	MOUSE	Bcl2	*Mus musculus*
sp|Q9JJV8|BCL2	CRIGR	BCL2	*Cricetulus griseus*
sp|P10415|BCL2	HUMAN	BCL2	*Homo sapiens*
tr|G8GLM0|G8GLM0	CAVPO	BCL2	*Cavia porcellus*
sp|O43521|B2L11	HUMAN	BCL2L11	*Homo sapiens*
sp|O88498|B2L11	RAT	Bcl2l11	*Rattus norvegicus*
sp|O54918|B2L11	MOUSE	Bcl2l11	*Mus musculus*
sp|P59017|B2L13	MOUSE	Bcl2l13	*Mus musculus*
sp|Q9BXK5|B2L13	HUMAN	BCL2L13	*Homo sapiens*
sp|Q92934|BAD	HUMAN	BAD	*Homo sapiens*
sp|Q61337|BAD	MOUSE	Bad	*Mus musculus*
sp|O35147|BAD	RAT	Bad	*Rattus norvegicus*
sp|P48558|BXI1	YEAST	Bax	*Saccharomyces cerevisiae*
sp|O74888|BXI1	SCHPO	Bax	*Schizosaccharomyces pombe*
sp|Q9Z0F3|B2L10	MOUSE	Bcl2l10	*Mus musculus*
sp|Q9BXH1|BBC3	HUMAN	BBC3	*Homo sapiens*
sp|Q80ZG6|BBC3	RAT	Bbc3	*Rattus norvegicus*
sp|Q99ML1|BBC3	MOUSE	Bbc3	*Mus musculus*
sp|Q13323|BIK	HUMAN	BIK	*Homo sapiens*
sp|O70337|BIK	MOUSE	Bik	*Mus musculus*
sp|Q07813|BAX	MOUSE	BAX	*Mus musculus*
tr|G5BAG6|G5BAG6	HETGA	BAX	*Heterocephalus glaber*
sp|Q07812|BAX	HUMAN	BAX	*Homo sapiens*
sp|O02703|BAX	BOVIN	BAX	*Bos Taurus*
tr|Q8SQ43|Q8SQ43	FELCA	BAX	*Felis catus*
sp|O00198|HRK	HUMAN	HRK	*Homo sapiens*
sp|P97287|MCL1	MOUSE	Mcl1	*Mus musculus*
sp|Q9Z1P3|MCL1	RAT	Mcl1	*Rattus norvegicus*
sp|Q07820|MCL1	HUMAN	MCL1	*Homo sapiens*
sp|Q7YRZ9|MCL1	FELCA	MCL1	*Felis catus*
sp|Q8HYS5|MCL1	CANFA	MCL1	*Canis familiaris*
tr|Q1LX52|Q1LX52	DANRE	BID	*Danio rerio*
tr|Q56VD1|Q56VD1	XENLA	BID	*Xenopus laevis*
tr|A0SZK2|A0SZK2	XENTR	BID	*Xenopus tropicalis*
tr|V8P747|V8P747	OPHHA	BID	*Ophiophagus hannah*
sp|Q8JGM8|BID	CHICK	BID	*Gallus gallus*
tr|U6D381|U6D381	NEOVI	BID	*Neovison vison*
sp|Q4JHS0|BID	PIG	BID	*Sus scrofa*

tr|Q05KI6|Q05KI6	BOVIN	BID	*Bos Taurus*
tr|Q17QH5|Q17QH5	BOVIN	BID	*Bos Taurus*
sp|P70444|BID	MOUSE	BID	*Mus musculus*
sp|Q9JLT6|BID	RAT	BID	*Rattus norvegicus*
tr|A8ASI9|A8ASI9	RAT	BID	*Rattus norvegicus*
tr|E2IV85|E2IV85	FELCA	BID	*Felis catus*
tr|E2IV86|E2IV86	LEMCA	BID	*Lemur catta*
tr|B2ZP78|B2ZP78	HUMAN	BID	*Homo sapiens*
sp|P55957|BID	HUMAN	BID	*Homo sapiens*
tr|A8ASI8|A8ASI8	HUMAN	BID	*Homo sapiens*
tr|E2IV87|E2IV87	9PRIM	BID	*Saimiri boliviensis*
tr|E2IV84|E2IV84	AOTVO	BID	*Aotus vociferans*
sp|Q6GP52|BECN1	XENLA	Beclin-1	*Xenopus laevis*
sp|Q4A1L3|BECN1	XENTR	Beclin-1	*Xenopus tropicalis*
sp|Q5ZKS6|BECN1	CHICK	Beclin-1	*Gallus gallus*
sp|Q14457|BECN1	HUMAN	Beclin-1	*Homo sapiens*
sp|Q5R878|BECN1	PONAB	Beclin-1	*Pongo abelii*
sp|Q91XJ1|BECN1	RAT	Beclin-1	*Rattus norvegicus*
sp|O88597|BECN1	MOUSE	Beclin-1	*Mus musculus*
sp|Q4A1L5|BECN1	PIG	Beclin-1	*Sus scrofa*
sp|Q4A1L4|BECN1	BOVIN	Beclin-1	*Bos Taurus*

Supplemental references

Aon MA, Cortassa S, Wei AC, Grunnet M, O'Rourke B (2010) Energetic performance is improved by specific activation of K+ fluxes through K(Ca) channels in heart mitochondria. *Biochim Biophys Acta* **1797:** 71-80

Foster DB, Ho AS, Rucker J, Garlid AO, Chen L, Sidor A, Garlid KD, O'Rourke B (2012) Mitochondrial ROMK channel is a molecular component of mitoK(ATP). *Circ Res* **111:** 446-454

Garlid KD, DiResta DJ, Beavis AD, Martin WH (1986) On the mechanism by which dicyclohexylcarbodiimide and quinine inhibit K+ transport in rat liver mitochondria. *J Biol Chem* **261:** 1529-1535

Le SQ, Gascuel O (2008) An improved general amino acid replacement matrix. *Mol Biol Evol* **25:** 1307-1320

Martin WH, DiResta DJ, Garlid KD (1986) Kinetics of inhibition and binding of dicyclohexylcarbodiimide to the 82,000-dalton mitochondrial K+/H+ antiporter. *J Biol Chem* **261:** 12300-12305

Redelings BD, Suchard MA (2007) Incorporating indel information into phylogeny estimation for rapidly emerging pathogens. *BMC Evol Biol* **7:** 40

Saitou N, Nei M (1987) The neighbor-joining method: a new method for reconstructing phylogenetic trees. *Mol Biol Evol* **4:** 406-425

Tamura K, Battistuzzi FU, Billing-Ross P, Murillo O, Filipski A, Kumar S (2012) Estimating divergence times in large molecular phylogenies. *Proc Natl Acad Sci U S A* **109:** 19333-19338

Tamura K, Stecher G, Peterson D, Filipski A, Kumar S (2013) MEGA6: Molecular Evolutionary Genetics Analysis version 6.0. *Mol Biol Evol* **30:** 2725-2729